Supporting Information

Anionic engineering of a p-dopant enables efficient and stable perovskite solar cells

Correspondence to: luojs@uestc.edu.cn

Table of Contents

1. Materials

FAI (99.8%) were purchased from Greatcell Solar. PbI_2 (99.999%) and ITO glass were purchased from Advanced Election Technology CO., Ltd. PTAA (99.9%), Spiro-OMeTAD (99.9%), *t*-BP (99%), $PbBr_2$ (99.9%), MABr (99.8%) and CsBr (99.9%) were purchased from Xi'an Yuri Solar Co.,Ltd. Lithium tetrakis(pentafluorophenyl)borate ethyl etherate (Li-BCF) was purchased from J&K Scientific. The SnO_2 (15 wt%) was purchased from Alfa Aesar. The N, N-dimethylformamide (DMF, 99.9%), Li-TFSI (99%), dimethyl sulfoxide (DMSO, 99.9%), chlorobenzene, isopropanol (IPA, 99.9%) and acetonitrile were purchased from Sigma-Aldrich. Ethanol was purchased from Aladdin. All the materials were used as received without any purification.

2. Characterization

The ultraviolet-visible absorption spectrum (UV-vis) was measured by a Hitachi UV-visible spectrophotometer (U-2910). The electron spin resonance spectroscopy (ESR) was analyzed by a Bruker-E500 spectrometer. The ultraviolet photoelectron spectroscopy (UPS) measurements were performed by the AXIS ULTRA DLD instrument from Kratos, UK, using a HeI monochromator with 21.22 eV source energy. The steady-state fluorescence spectroscopy (PL) was collected by a Hitachi spectrophotometer (F-4600). The transient fluorescence spectra (TRPL) were measured at room temperature using the time-correlated single photon counting (TCSPC) technique with a FluoroLog-3 modular spectrofluorometer (HORIBA Jobin Yvon). The

electrochemical impedance spectroscopy (EIS) of the PSCs under ambient air was recorded by an electrochemical workstation (CHI 660E, Shanghai, Chenhua) and a solar simulator (Zolix Instrument Co., Ltd. Beijing). The surface and cross-sectional morphology of the films were observed by a scanning electron microscopy (JEOL JSM-7600F). The *J-V* curve of the PSCs was measured at room temperature using an electrochemical workstation (CHI 660E, Shanghai, Chenhua) under AM 1.5G simulated solar light (100 mW cm^{-2}), and the incident light intensity was calibrated with a standard silicon solar cell. Incident photon-to-electron conversion efficiency (IPCE) spectrum was measured using a CROWNTECH, QTest Station 2000 IPCE testing system. Regarding the environmental stability of the PSCs, the devices were kept at ambient conditions (50-85% room humidity and room temperature) in a dark environment for 30 days. Regarding the operational stability of PSCs, unencapsulated PSCs were continuously tested in a standard LED simulated sunlight, room temperature and N_2 atmosphere. The water contact angle of the films was examined by a droplet shape analyzer (Krüss DSA100). The atomic force microscopy (AFM) measured by Bruker Dimension Icon AFM instrument. Two dimensional grazing incidence X-ray diffraction (2D-GIXD) images were conducted at BL14B1 beamline of Shanghai Synchrotron Radiation Facility (SSRF) (λ = 1.24 Å). The incidence angle is 0.16 degree and the exposure time is 60 s. Time-of-flight secondary-ion mass spectrometry (TOF-SIMS) was performed by TOF.SIMS 5 (IONTOF GmbH, Germany). A dual-beam TOF-

SIMS was used with Cs^+ primary ions (0.5 keV, 26 nA, 300 × 300 μm^2) for the erosion and a Bi^+ pulsed primary ion beam for the analysis of anion (30 keV, 1 pA, 100 × 100 μm^2).

3. DFT calculations

Electrostatic potential (ESP) calculations utilized the Gaussian16, A.03 software package. For geometry optimizations, the B3LYP functional[1] was employed in conjunction with the Becke-Johnson damping scheme (D3BJ)[2, 3]. All atoms were modeled using the 6-31G(d,p) basis set[4].

Calculation related to molecular orbitals were performed in the DFT framework carried out by the Dmol3 program[5] with a Generalized Gradient Approximation-Perdew Burke Ernzerh (GGA-PBE) exchange correlation functional[6]. The self-consistent field (SCF) convergence criterion of 1 × 10^{-6} Ha was adopted to the geometry optimization, and the total energy convergence tolerance and force tolerance were set to be 1 × 10^{-5} Ha, 2 × 10^{-3} Ha $Å^{-1}$, respectively.

The CP2K program[7] was utilized for the calculations of relaxed models, electron transfer, and other optimized structures, employing the spin-polarized density functional theory[8, 9]. A mixed Gaussian and plane-wave basis set was applied for all calculations. Core electrons were represented using norm-conserving Goedecker-Teter-Hutter pseudopotentials[10-12], and van der Waals interactions were corrected using Grimme's DFT-D3 model[2]. The exchange-correlation functional was GGA-PBE. Valence electron wavefunctions were

expanded using a double-zeta basis set with polarization functions[13], supplemented by an auxiliary plane-wave basis set with an energy cutoff of 360 eV. Configurations were optimized via the Broyden-Fletcher-Goldfarb-Shanno (BGFS) algorithm, achieving a self-consistent field (SCF) convergence criterion of 1.0×10^{-6} au.

4. Precursor solution and device fabrication

The ITO glass substrates were ultrasonically cleaned with deionized water, acetone, and ethanol in sequence, each step was more than 30 minutes, and dried with a nitrogen flow, then treated with UV-ozone for 30 minutes. All the solutions were passed through a 0.22-mmfilter before use. The SnO_2 solution was prepared by diluting 15 wt% SnO_2 aqueous solutions (400 μL) with 1.1 mL of isopropanol/H_2O (1/1, v/v). The SnO_2 solution was spin coated onto an ITO substrate at 3000 rpm for 30 s, and annealed in ambient air at 150 °C for 30 min. 1.2 M $Cs_{0.05}FA_{0.85}MA_{0.1}Pb(I_{0.95}Br_{0.05})_3$ perovskite precursor solution was prepared in mixture solvent of DMF and DMSO (4:1, v/v). The perovskite solution was spin coated with t a one-step spin-coating process at 1300 rpm for 10 s and 5000 rpm for 45 s, respectively. The spin-coated perovskite precursor films were sequentially heated at 110 °C. For the control PTAA: Li-TFSI solution, dissolved 15 mg PTAA in 1 mL of chlorobenzene, added 7.5 μL of bis(trifluoromethane)sulfonamide lithium salt (Li-TFSI)/acetonitrile (170 mg/mL) and 7.5 μL of *t*-BP/acetonitrile (1:1 v/v). The PTAA and Li-BCF were dissolved into 1 mL CB and mixed by desired Li-BCF/PTAA ratios 5% to 10% (weight

ratio). For the control Sprio-OMeTAD: Li-TFSI solution, dissolved 72.3 mg Sprio-OMeTAD in 1 mL of chlorobenzene, added 17.5 μL of Li-TFSI/acetonitrile (520 mg/mL) and 28.8 μL of t-BP. The Sprio-OMeTAD and Li-BCF were dissolved into 1 mL CB and mixed by desired Li-BCF/Sprio-OMeTAD ratios 2% to 10% (weight ratio). The HTL solution was spin-coated on the perovskite layer by spin coating at 3000 rpm for 30 s. Finally, Au electrode was thermally evaporated.

5. Figures S1-S11

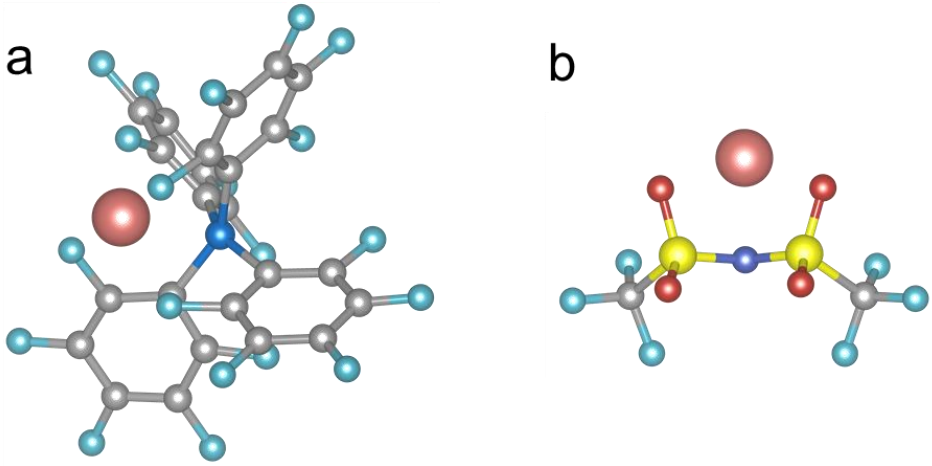

Figure S1. Density functional theory (DFT) calculation results. Optimized structures of (a) Li-BCF and (b) Li-TFSI.

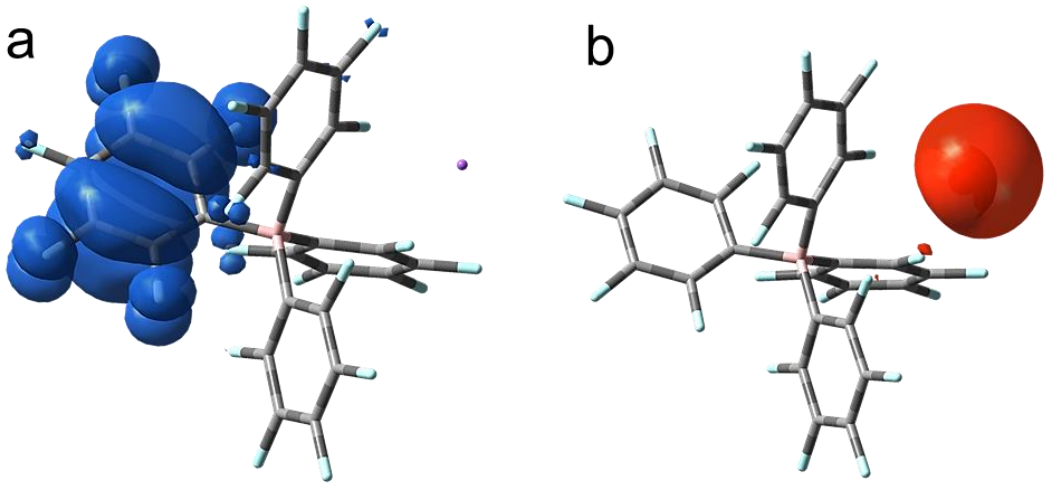

Figure S2. Density functional theory (DFT) calculation results**.** (a) HOMO and (b) LUMO density of Li-BCF.

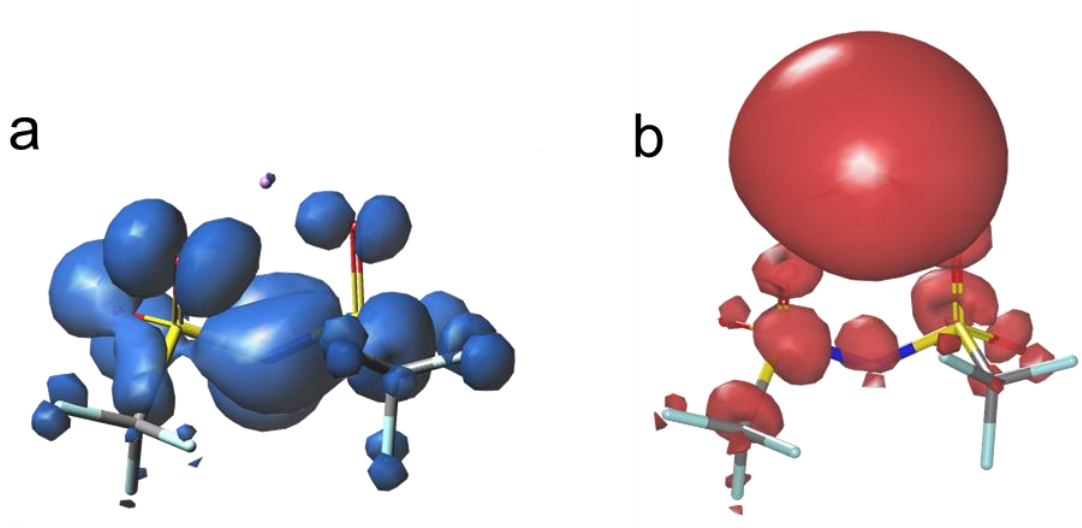

Figure S3. Density functional theory (DFT) calculation results. (a) HOMO and (b) LUMO density of Li-TFSI.

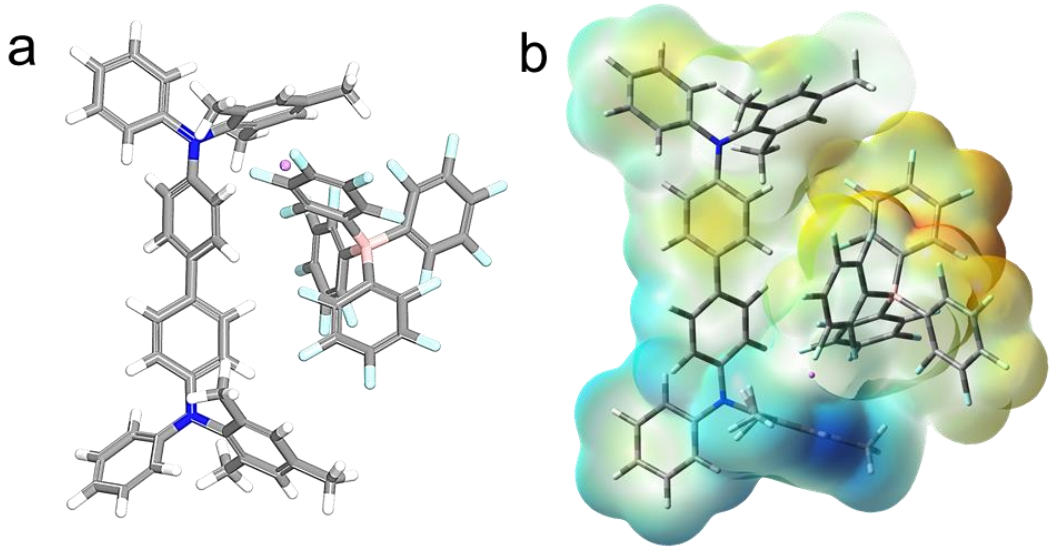

Figure S4. Density functional theory (DFT) calculation results. (a) Optimized structure of the Li-BCF/PTAA dimer interaction model and (b) its corresponding Electrostatic potential (ESP) surface.

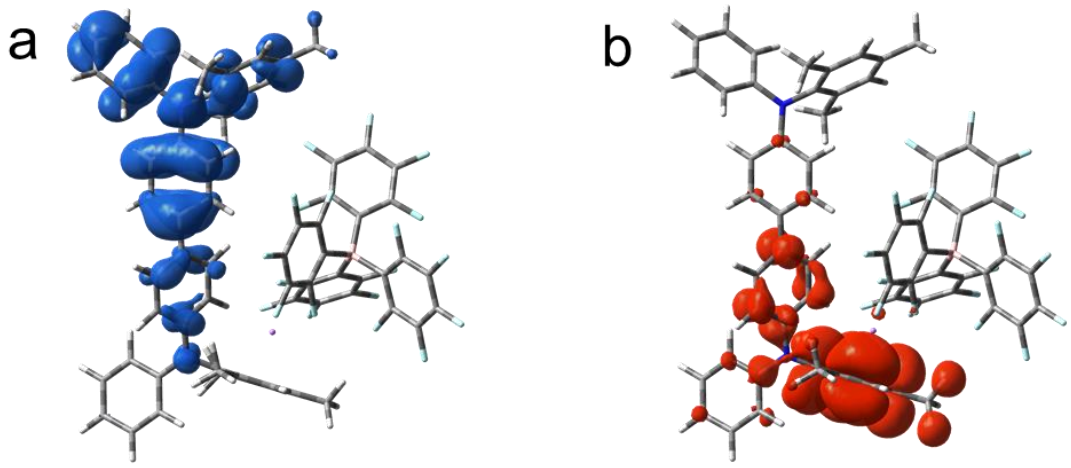

Figure S5. Density functional theory (DFT) calculation results. (a) HOMO and (b) LUMO density of Li-BCF/PTAA dimer interaction model.

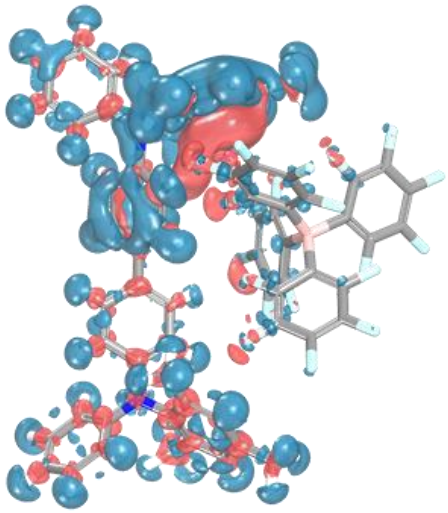

Figure S6. Density functional theory (DFT) calculation results. Differential charge map of Li-BCF/PTAA interaction model (red and blue respectively represent the accumulation and depletion of electrons).

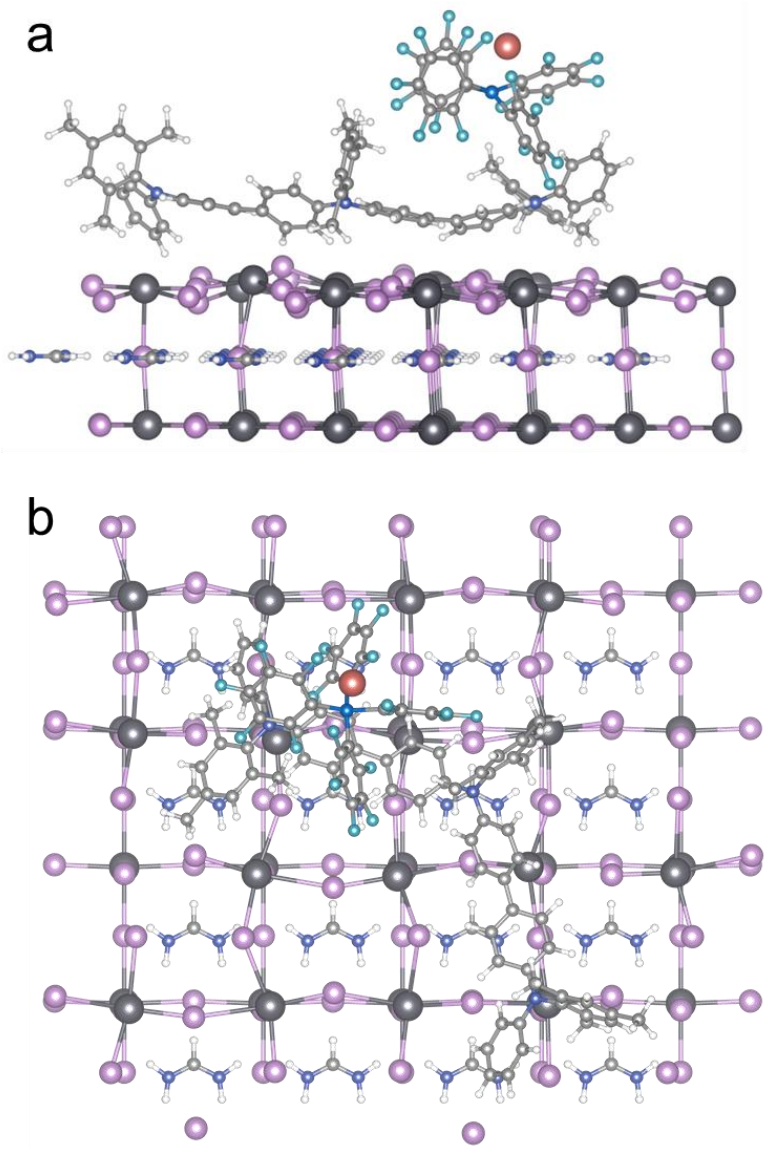

Figure S7. Density functional theory (DFT) calculation results. (a) Side view and (b) top view of the optimized model of Li-BCF/ PTAA trimer/ PVK lattice.

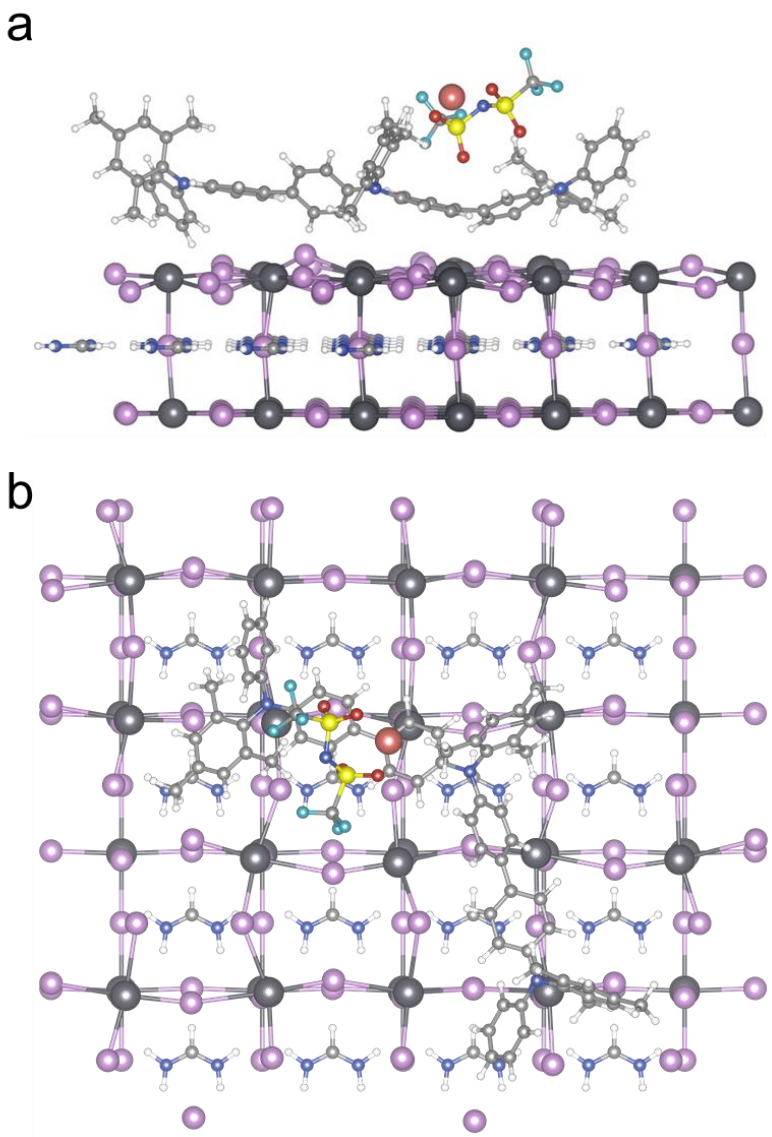

Figure S8. Density functional theory (DFT) calculation results. (a) Side view and (b) top view of the optimized model of Li-TFSI/ PTAA trimer/ PVK lattice.

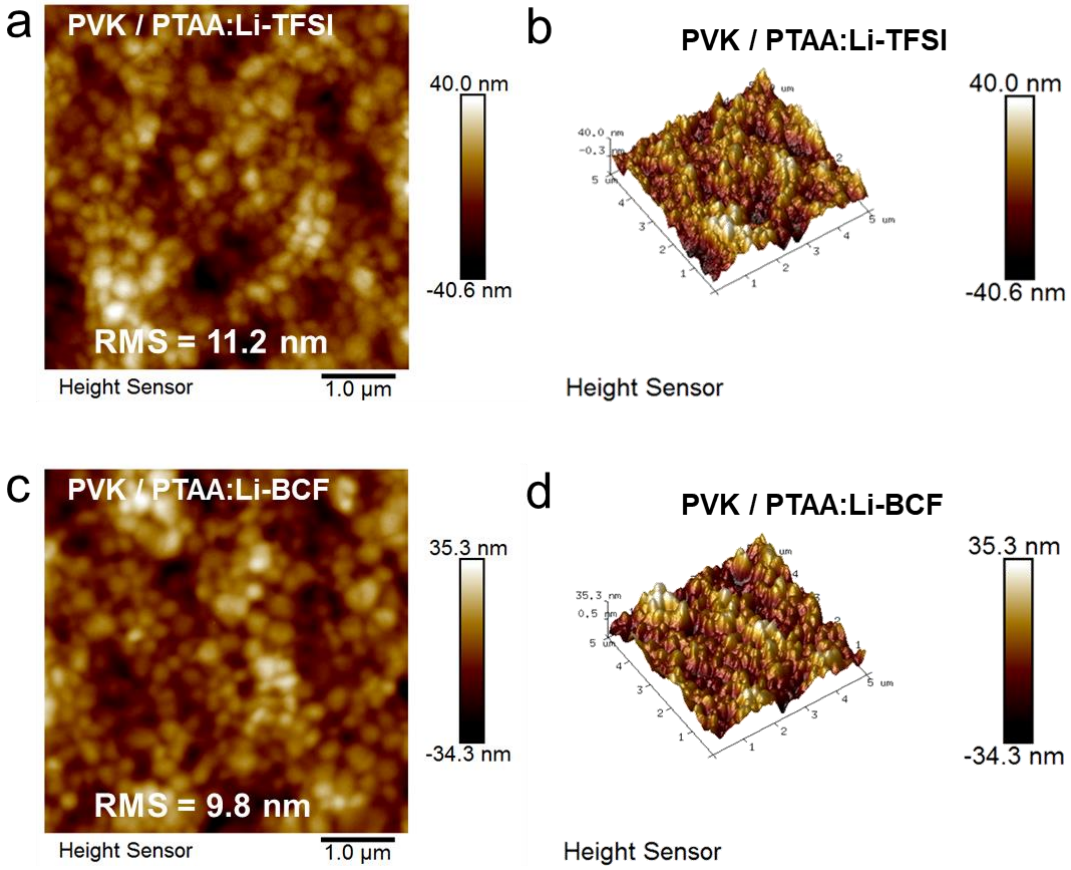

Figure S9. Tapping-mode AFM height and phase images (5 × 5 µm) of perovskite capped with (a, b) Li-TFSI doped PTAA film and (c, d) Li-BCF doped PTAA film respectively.

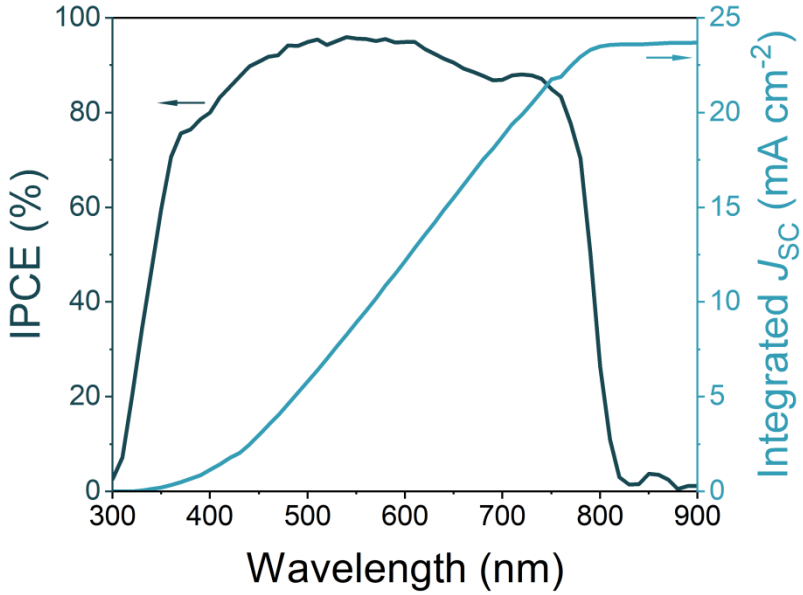

Figure S10. IPCE spectrum and integrated J_{SC} of Li-BCF doped photovoltaic device.

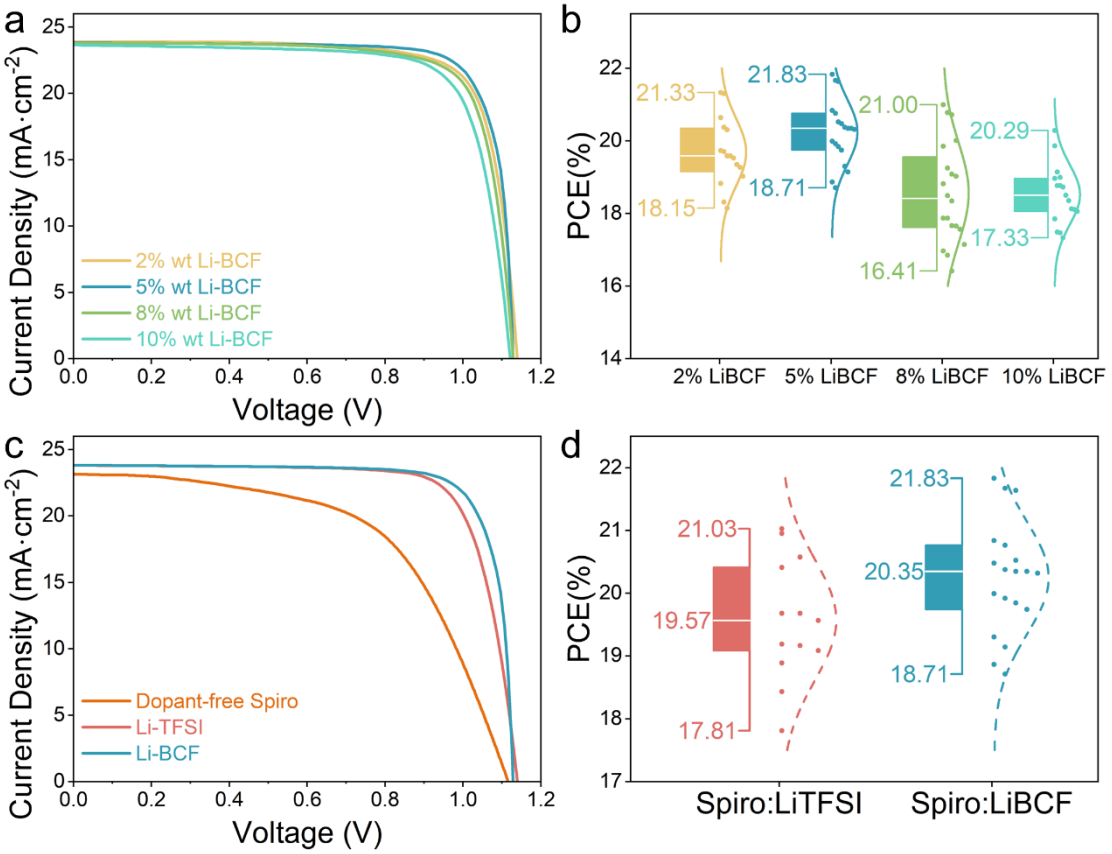

Figure S11. (a) Best *J-V* curves of Spiro-OMeTAD based PSCs and (b) the corresponding PCE box plot with different doping concentrations of Li-BCF (2 wt%, 5 wt%, 8 wt%, 10 wt%). (c) Best *J-V* curves and (d) the corresponding PCE box plot of Spiro-OMeTAD devices under different doping systems. The numbers in the box plot from top to bottom are the maximum, median, and minimum values, respectively.

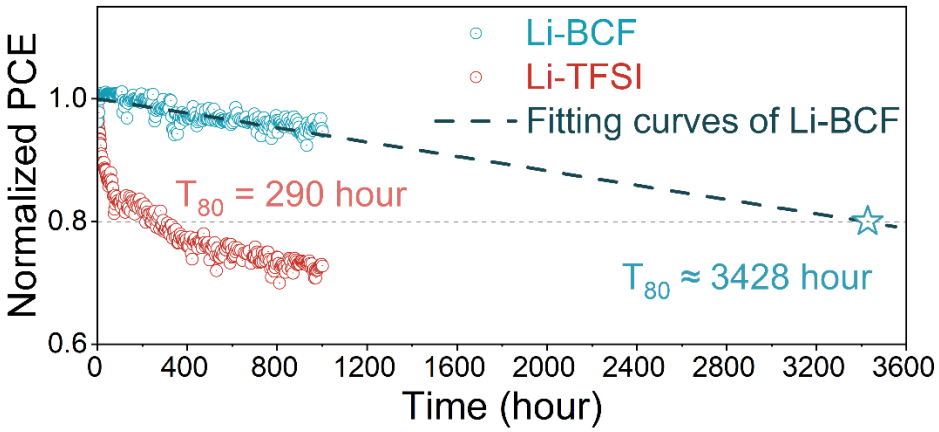

161

162 **Figure S12.** The fitting curve for Li-BCF operational stability data, with detailed

163 fitting parameters shown in Table S2.

164

165

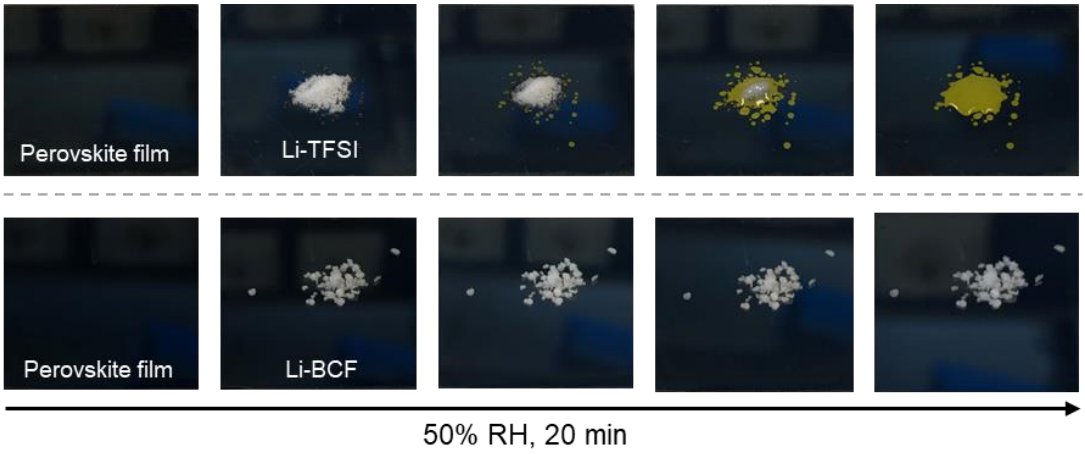

166

167 **Figure S13.** Photos of dopants decomposing perovskite films by absorbing

168 moisture in the air.

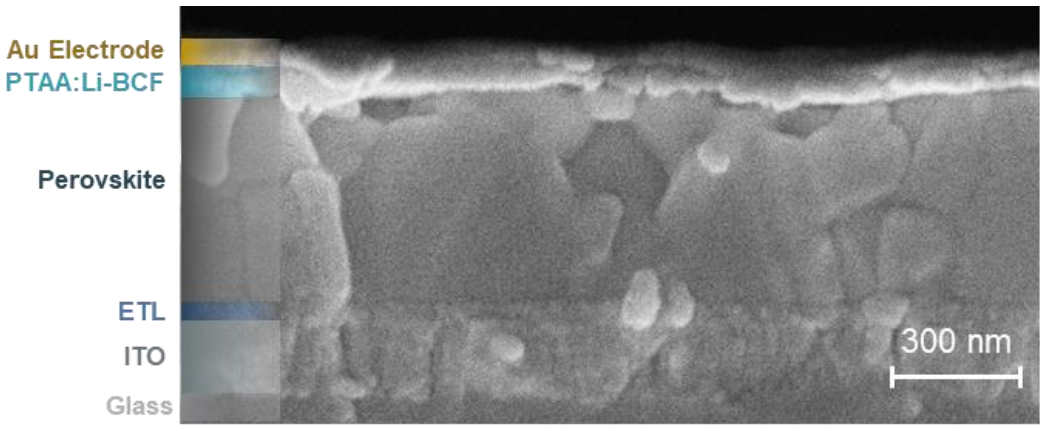

Figure S14. Cross-sectional SEM image of aged Li-BCF-doped device (20 days, 25 °C, 50-85% RH).

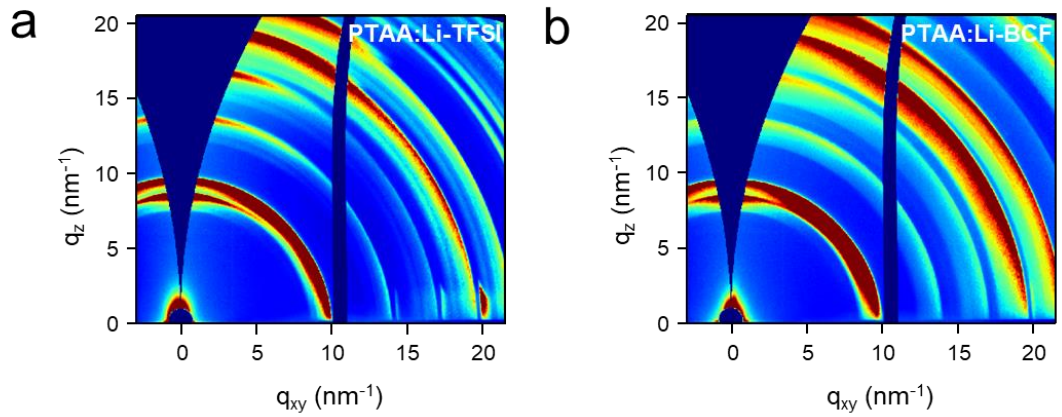

Figure S15. 2D-GIXD data of aged PSCs based on (a) PTAA:Li-TFSI and (b) PTAA:Li-BCF under the ambient conditions without encapsulation for 30 days.

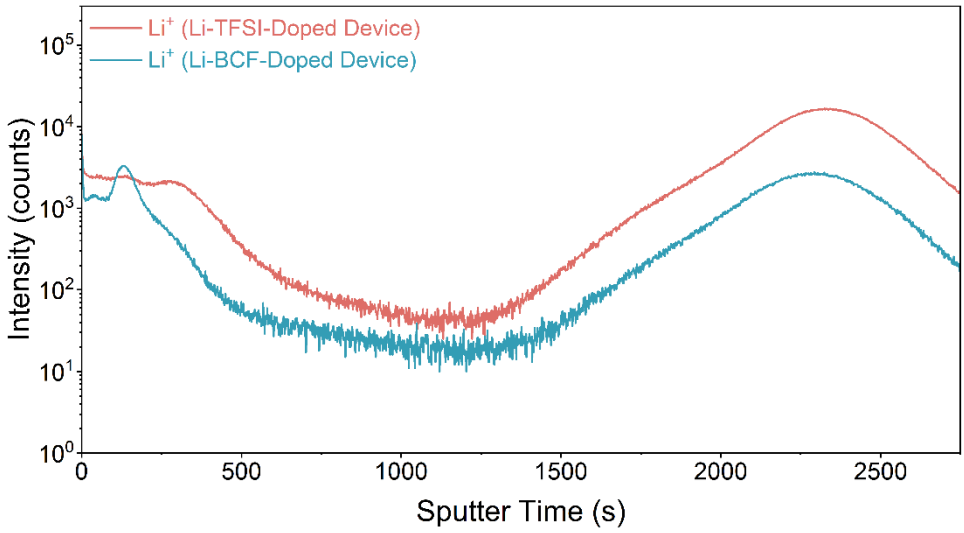

175

176 **Figure S16.** TOF-SIMS results of Li^+ ions in aged devices based on Li-TFSI

177 and Li-BCF.

6. Table S1-3

Table S1. The fitting parameters of TRPL data through an exponential model.

Sample	A_1	τ_1 (ns)	A_2	τ_2 (ns)	τ_{ave} (ns)
Perovskite	0.46	69.01	0.45	395.08	345.68
Perovskite/PTAA	0.64	8.80	0.38	67.05	56.51
Perovskite/PTAA: Li-TFSI	1.45	2.65	0.34	21.88	15.33
Perovskite/PTAA: Li-BCF	2.52	1.77	0.34	14.62	8.54

Table S2. Summary of the photovoltaic parameters of Spiro-OMeTAD based PSCs with different doping system.

Doping system	J_{SC} (mA cm^{-2})	V_{OC} (V)	FF (%)	PCE (%)
Dopant-free Spiro-OMeTAD	23.20	1.116	57.16	14.80
Spiro-OMeTAD: Li-TFSI	23.81	1.139	77.55	21.03
Spiro-OMeTAD: 2 wt% Li-BCF	23.89	1.138	78.46	21.33
Spiro-OMeTAD: 5 wt% Li-BCF	23.82	1.129	81.17	21.83
Spiro-OMeTAD: 8 wt% Li-BCF	23.77	1.128	78.32	21.00
Spiro-OMeTAD: 10 wt% Li-BCF	23.65	1.121	76.53	20.29

184

185 **Table S3.** The fitting parameters of Li-BCF operational stability data through an

186 linear model.

Fitting Parameter	
Equation	PCE(t) = a + b t
Weight	Unweighted
Intercept (a)	$1.00 \pm 9.51 \times 10^{-4}$
Slope (b)	$-5.86 \times 10^{-5} \pm 1.79 \times 10^{-6}$
Sum of Squares of Residuals	0.029
Pearson's r	-0.88
Coefficient of Determination	0.78

187

References

1 P. J. Stephens, F. J. Devlin, C. F. Chabalowski and M. J. Frisch, *The Journal of Physical Chemistry*, 1994, **98**, 11623-11627.

2 S. Grimme, J. Antony, S. Ehrlich and H. Krieg, *J Chem. Phys.*, 2010, **132**, 154104.

3 S. Grimme, S. Ehrlich and L. Goerigk, *J. Comput. Chem.*, 2011, **32**, 1456-1465.

4 Y. Zhao and D. G. Truhlar, *Theor. Chem. Acc.*, 2008, **120**, 215-241.

5 B. Delley, *J Chem. Phys.*, 1990, **92**, 508-517.

6 B. Delley, *J Chem. Phys.*, 2000, **113**, 7756-7764.

7 J. VandeVondele, M. Krack, F. Mohamed, M. Parrinello, T. Chassaing and J. Hutter, *Comput. Phys. Commun.*, 2005, **167**, 103-128.

8 P. Hohenberg and W. Kohn, *Phys. Rev.*, 1964, **136**, B864-B871.

9 W. Kohn and L. J. Sham, *Phys. Rev.*, 1965, **140**, A1133-A1138.

10 S. Goedecker, M. Teter and J. Hutter, *Phys. Rev. B*, 1996, **54**, 1703-1710.

11 C. Hartwigsen, S. Goedecker and J. Hutter, *Phys. Rev. B*, 1998, **58**, 3641-3662.

12 M. Krack and M. Parrinello, *Phys. Chem. Chem. Phys.*, 2000, **2**, 2105-2112.

13 J. VandeVondele and J. Hutter, *J Chem. Phys.*, 2007, **127**, 114105.